CRYSTAL GROWTH & DESIGN

pubs.acs.org/crystal

Article

Molecular-Level Investigation of Hydrate−Anhydrous Phase Transformations of the Dapsone Structurally Related Compound 3,3′-Diaminophenyl Sulfone

Paola Paoli, Martina Lippi, Stella Milazzo, Patrizia Rossi,* Jacopo Ceccarelli, Laura Chelazzi, Andrea Ienco, and Luca Conti

Cite This: *Cryst. Growth Des.* 2022, 22, 7176−7186

Read Online

ACCESS | Metrics & More | Article Recommendations | Supporting Information

ABSTRACT: The solid state of a novel hydrate form of 3,3′-diaminophenyl sulfone (**3APS_0.5H$_2$Oo**) as well as its temperature-induced phase transitions is reported. On increasing the temperature, first a partial dehydration occurs, leading to the partially hydrated **3APS_0.1H$_2$Oo**, which then transforms into the monoclinic anhydrous form, **3APS_Am**. Finally, by recrystallization of the melt **3APS_Am**, a second anhydrous orthorhombic phase is obtained (**3APS_Ao**). This last phase transforms in **3APS_Am** at a temperature between 360 and 400 K. XRD, DSC, TGA, HSM, and *in silico* data have been used to better understand the dehydration mechanism. With the same aim, hydration/dehydration tests have been carried out. Finally, the dehydration behavior of **3APS_0.5H$_2$O** has been discussed in comparison with that of the dapsone hydrated phase **4APS_0.33H$_2$Om**.

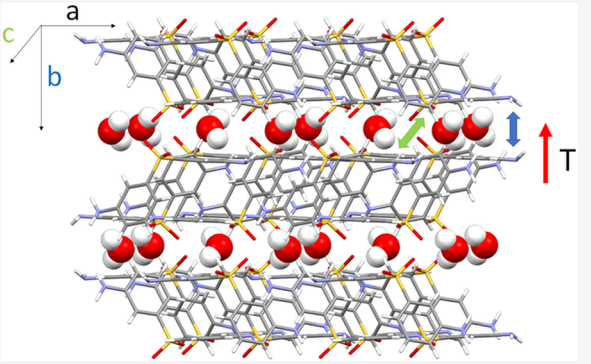

INTRODUCTION

Organic sulfones are an important class of compounds that find different applications as for example in medicinal chemistry,[1] electronics,[2] and organic synthesis as well[3] due to their manifold reactivity. The anti-HIV activity of sulfones was discovered in 1993 following a large-scale drug screening. Mc Mohan et al. reported the inhibition of HIV-1 reverse transcription by various diaryl sulfones, making them a new emerging class of non-nucleoside reverse transcriptase inhibitors.[4] Aryl sulfones were also studied as γ-secretase inhibitors for the potential treatment of Alzheimer's disease.[5] Furthermore, aryl sulfone-based B1 antagonists show improved efficacy when compared to sulfonamide for the treatment of chronic pain.[6] 4,4′-Diaminophenyl sulfone, better known as dapsone (4APS, in the following), is a milestone among antibiotic drugs due to its effectiveness in the treatment of leprosy, dermatitis herpetiformis, malaria, and tuberculosis.[7] More recently, dapsone has been investigated for its potential survival benefit in patients hospitalized with COVID-19.[8]

Finally, dapsone is also an interesting molecule from a solid-state point of view since its rich solid forms variety, which comprises several anhydrates and solvates and one hydrate.[9,10] The structurally related 3,3′-diaminophenyl sulfone, $C_{12}H_{12}N_2O_2S$ (3APS in the following, Scheme 1), which differs in the relative position of the amine group on the aromatic ring, is also an interesting molecule. For example, 3APS (as well as dapsone) silver coordination polymers show luminescent properties, so they are of interest because of their potential applications in chemical sensors, photochemistry, and electroluminescent displays.[11] Other applications of 3APS vary from the preparation of analogues of Congo red[12] and hybrid organic−inorganic materials.[13−15]

Scheme 1. Schematic Drawing of 3APS

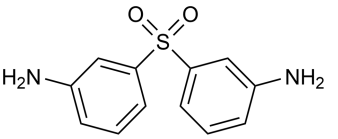

Interestingly, although the structural similarity between 3APS and dapsone could make it possible to foresee for the first compound the existence of a rich variety of solid forms (the neutral dapsone molecule has five polymorphs), only one crystal phase containing neutral 3APS molecules is known. The crystal structure of 3APS was first characterized in 2008 by Ghazisaeidi and Yousefi[16] (ROMCAY refcode in the Cambridge Structural Database, version 5.42 update Sep 21)[17] and then investigated again in 2010 in a comparative study about diphenyl sulfones

Received: July 27, 2022
Revised: October 20, 2022
Published: November 3, 2022

Table 1. Crystallographic Data and Refinement Parameters for 3APS_0.5H_2Oo, 3APS_0.1H_2Oo, and 3APS_Am (100 and 360 K)[a]

	3APS_0.5H_2Oo	3APS_0.1H_2Oo	3APS_Am	
empirical formula	$C_{12}H_{12}N_2O_2S{\cdot}0.5H_2O$	$C_{12}H_{12}N_2O_2S{\cdot}0.1H_2O$	$C_{12}H_{12}N_2O_2S$	
formula weight	257.30	250.10	248.30	
T (K)	100	350	100	360
crystal system, space group	orthorhombic, *Pbna*	orthorhombic, *Pbna*	Monoclinic, $P2_1/c$	
unit-cell dimensions (Å, °)	a = 10.018(3)	a = 9.8452(7)	a = 8.6204(5)	a = 8.631(2)
	b = 14.108(3)	b = 14.485(1)	b = 8.6781(5); β = 97.171(4)	b = 8.819(2); β= 98.40(2)
	c = 17.075(4)	c = 17.024(1)	c = 15.7152(8)	c = 16.144(4)
V (Å^3)	2413(1)	2427.8(3)	1166.4(1)	1215.6(4)
Z, dcalc(g/cm^3)	8,1.416	8,1.368	4,1.414	4,1.357
μ (mm^{-1})	2.375	2.320	2.404	2.307
F (000)	1080	1048	520	520
reflections collected/unique/rint	24457/2469/0.0940	12958/2418/0.0571	8836/1895/0.0928	8158/2167/0.0738
data/parameters	2469/198	2418/192	1895/190	2167/155
final R indices [I>2σ(I)]	R_1 = 0.0476, wR_2 = 0.1345	R_1 = 0.0795, wR_2 = 0.2122	R_1 = 0.0625, wR_2 = 0.1671	R_1 = 0.0832, wR_2 = 0.2300
R indices of all data	R_1 = 0.0568, wR2 = 0.1440	R_1 = 0.0976, wR_2 = 0.2337	R_1 = 0.0867, wR_2 = 0.1978	R_1 = 0.1680, wR_2 = 0.3120
max/min residual Fourier density	0.51/−0.78	0.32/−0.63	1.13/−0.59	0.43/−0.32
GoF	1.115	1.050	1.063	1.080

[a]= data have been collected using Cu-Kα radiation (λ = 1.54184 Å).

that were structurally correlated (ROMCAY01).[18] 3APS crystallizes in the space group $P2_1/c$, with one independent molecule in the asymmetric unit (**3APS_Am**, hereafter). A search in the Cambridge Structural Database (CSD) also shows other forms containing neutral or protonated 3APS molecules: two anhydrous salt-cocrystals (RAFDUZ[14] and VEWFEK[15]), a true salt (IYIVIY),[19] a true solvate (RIZDEK),[20] and two hybrid organic−inorganic compounds (SUWVOY[21] and TEGGUK[13]).

With this in mind, we decided to investigate the solid form landscape of 3APS. In this context, X-ray diffraction (XRD), which includes single-crystal X-ray diffraction (SCXRD) and microcrystalline powder X-ray diffraction (PXRD), together with thermoanalytical techniques such as thermogravimetric analysis (TGA) and differential scanning calorimetry (DSC) as well as *in silico* studies are commonly used as interdisciplinary tools for a thorough solid-state investigation. In recent years, we have used this combined approach for studying the solid forms of active pharmaceutical ingredients (APIs), their salts, metal complexes, hydrates, and combinations thereof. In particular, valuable information on the molecular and crystal structures of the corresponding crystalline solids have been extracted[22] and correlated to their properties, *e.g.*, isotropic vs anisotropic thermal expansion,[23−25] chiral recognition,[26] phase stability/transformation,[27] solvation/desolvation processes,[28−30] and polymorphic behavior.[31−34]

In general, for crystalline molecular solids, multiple solid forms, and their interconversion tendency in response to chemical and/or physical stimuli such as heating, can be considered important tools to evaluate their physical−chemical property's versatility and thus manufacture high-quality compounds, especially for drug design and material chemistry.

During the solid form landscape investigation of 3APS, a hemihydrated species (**3APS_0.5H_2Oo**) was identified and characterized by SCXRD. The occurrence of the already known anhydrous species[16,18] prompted us to investigate the stability of the hemihydrated species with respect to the dehydration process at the molecular level, using a combined experimental (XRD, TGA, DSC, hot-stage microscopy) and computational approach. The environmental changes that promote the hydration−dehydration processes were also investigated.

The molecular and crystal structures of all of the crystalline forms have been discussed and compared to the literature data of the strictly related dapsone molecule.

EXPERIMENTAL SECTION

Materials. 3,3′-Diaminophenyl sulfone was purchased from Sigma-Aldrich (CAS Number 599-61-1). It was used as received without further purification. **3APS_Am** crystals of suitable SCXRD quality were obtained with the procedure reported in ref 18.

Preparation of 3APS_0.5H_2Oo. **3APS_0.5H_2Oo** was prepared according to the procedure used for the preparation of the dapsone 0.33 hydrate form.[35] Crystals of **3APS_0.5H_2Oo** were obtained by adding the anhydrous 3APS to Milli-Q water and heating the mixture to the boiling point. The hot, saturated solution was filtered, covered with a parafilm, and allowed to crystallize by spontaneous cooling to room temperature (∼293 K). After one day, colorless hexagonal crystals were formed.

A microcrystalline powder of **3APS_0.5H_2Oo** was also prepared as follows: a slurry of 3APS in water was stirred in the temperature range from 298 to 313 K for two days. Then, the suspension was allowed to dry at room temperature. The resulting powder was stored at ambient conditions.

Single-Crystal X-ray Diffraction (SCXRD). Single-crystal X-ray diffraction data were collected at 100 (**3APS_0.5H_2Oo**, **3APS_Am**), 350 (**3APS_0.1H2Oo**), and 360 K (**3APS_Am**) using Cu-Kα radiation (λ = 1.54184 Å) on a Bruker Apex-II diffractometer equipped with a CCD detector, controlled using APEX2 software.[36] An Oxford Cryostream was used to control the temperature of the crystals prior to data collection. Data integration and reduction were performed using Bruker SAINT software.[37] Absorption correction was performed with the program SADABS-2016/2.[38] The crystal structures were solved using the SIR-2004 package[39] and refined by full-matrix least squares against F^2 using all data (SHELXL-2018/3).[40] All of the non-hydrogen atoms were refined with anisotropic displacement parameters. All of the hydrogen atoms of **3APS_Am** were set in calculated positions and refined in accordance with the atoms to which they are bonded. The hydrogen atoms of **3APS_0.5H_2Oo** and **3APS_0.1H_2Oo**, with the exception of the water hydrogen atoms in this last structure that were not introduced in the refinement, were found in the Fourier difference map. Their coordinates were freely refined, while their thermal parameter was set in accordance with the one of the atom to which they are bonded.

Geometrical calculations were performed by PARST97,[41] and molecular plots were produced by the program ORTEP3,[42] Mercury

https://doi.org/10.1021/acs.cgd.2c00849
Cryst. Growth Des. 2022, 22, 7176−7186

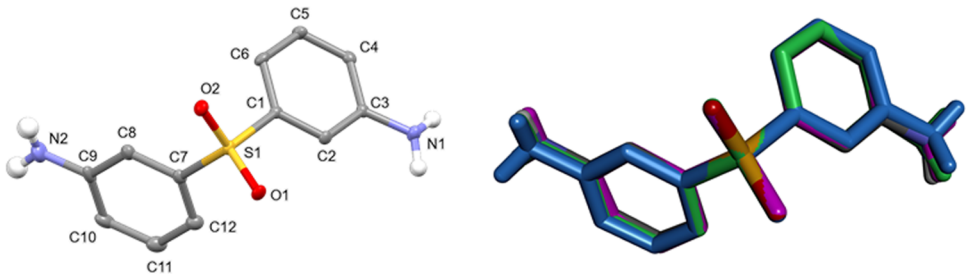

Figure 1. Left: Mercury view of 3APS in **3APS_Am** (100 K). Ellipsoids are drawn at 20% probability. Right: Superimposition of the 3APS molecule in the asymmetric unit of **3APS_Am** (100 K), **3APS_Am** (360 K, magenta), **3APS_0.5H$_2$Oo** (pale blue), and **3APS_0.1H$_2$Oo** (green).

Table 2. Selected Hydrogen Bonds in 3APS_0.5H$_2$Oo, 3APS_0.1H$_2$Oo, and 3APS_Am

	3APS_0.5H$_2$Oo			3APS_0.1H$_2$Oo		
X–H···Y	X···Y (Å)	H···Y (Å)	X–H···Y (°)	X···Y (Å)	H···Y (Å)	X–H···Y (°)
N1-H1na···O1w	3.017 (3)	2.13 (3)	165 (3)	3.00 (1)	2.11 (6)	155 (5)
O1w-H1wa···N2[a]	3.000 (2)	2.12 (3)	164 (3)	2.853 (7)[e]		
N1-H1nb···O1[b]	3.097 (3)	2.24 (4)	172 (3)	3.187 (6)	2.34 (7)	172 (6)
N2-H2na···N1[c]	3.174 (3)	2.27 (3)	164 (3)	3.316 (7)	2.34 (6)	159 (5)
N2-H2nb···O2[d]	3.106 (2)	2.25 (3)	159 (3)	3.226 (5)	2.26 (6)	174 (5)
	3APS_Am					
	100 K			360 K		
X–H···Y	X···Y (Å)	H···Y (Å)	X-H···Y (°)	X···Y (Å)	H···Y (Å)	X-H···Y (°)
N1-H1na···O2[f]	3.141 (5)	2.31 (4)	167 (3)	3.191 (7)	2.269 (5)	157.5 (4)
N1-H1na···O1[f]	3.706 (4)	3.02 (3)	140 (3)	3.684 (7)	2.996 (4)	137.5 (4)
N1-H1nb···O1[g]	3.039 (5)	2.25 (3)	157 (2)	3.087 (8)	2.303 (5)	150.0 (4)
N2-H2na···O1[h]	3.599 (5)	3.04 (5)	127 (4)	3.636 (9)	2.975 (4)	134.3 (5)
N2-H2na···N1[i]	3.317 (6)	2.69 (5)	132 (3)	3.47 (1)	2.808 (6)	133.8 (5)
N2-H2nb···O2[j]	3.040 (6)	2.27 (4)	152 (4)	3.136 (9)	2.287 (5)	164.9 (6)

[a] = 1 − *x*, 1 − *y*, 1 − *z*. [b] = −0.5+ *x*, *y*, 0.5 − *z* (**3APS_0.5H$_2$Oo**)/−0.5 + *x*, *y*, 1.5 − *z* (**3APS_0.1H$_2$Oo**). [c] = 1 + *x*, *y*, *z*. [d] = 2 − *x*, −0.5 + *y*, *z* (**3APS_0.5H$_2$Oo**)/−2 + *x*, 0.5 + *y*, *z* (**3APS_0.1H$_2$Oo**). [e] = only the *X*···*Y* distance was reported because the hydrogen atoms of the water molecule were not introduced in the refinement of **3APS_0.1H$_2$Oo**. [f] = −1 + *x*, *y*, *z*. [g] = 1 − *x*, 2 − *y*, 1 − *z*. [h] = *x*, −1 + *y*, *z*. [i] = 1 + *x*, −1 + *y*, *z*. [j] = 2 − *x*, −0.5 + *y*, 1.5 − *z*.

(v4.1.2),[43] and Discovery Studio Visualizer 2019.[44] Crystallographic data and refinement parameters are reported in Table 1. In Figure 1, an Ortep-3 view of 3APS in **3APS_Am** (100 K), as well as the superimposition of the 3APS molecule in **3APS_Am** (100 and 360 K), **3APS_0.5H$_2$Oo** (100 K), and **3APS_ 0.1H$_2$Oo** (350 K), has been reported.

X-ray Powder Diffraction (PXRD). *Room-Temperature Experiments.* Powder X-ray diffraction data were collected, at room temperature, in air using a Bruker New D8 Da Vinci diffractometer (Cu-Kα1 radiation = 1.54056 Å, 40 kV × 40 mA), equipped with a Bruker LYNXEYE-XE detector, in the scanning range 2θ = 3−40°, 0.02° with increments of 2θ and a counting time of 0.8 s/step.

Variable-Temperature (VT-PXRD) Experiments. Temperature-resolved experiments (performed in triplicates) were carried out in air in the 300−440 K range with an Anton Paar HTK 1200N hot chamber mounted on a Panalytical XPERT PRO diffractometer (Cu-Kα radiation, 40 kV × 40 mA), equipped with the PIX-CEL solid-state fast detector. The scanning range was 2θ= 4−40° with an 8 s/step counting time and 0.03° increments of 2θ. The temperature variation rate was 10 K/min; when the target temperature was reached, the sample was kept for 5 min at that temperature before collecting the data.

The crystal lattice parameters of **3APS_Am** at different temperatures were refined by a Rietveld refinement using the GSAS II[45] suite using the structural model of ROMCAY.[16] A shifted Chebyshev polynomial with eight coefficients, four-order spherical harmonic, and a pseudo-Voigt function were used to fit the background, the preferred orientation, and the peak shape, respectively. Unit-cell parameters and volume for **3APS_Am** are summarized in Table S1.

Finally, powder pattern indexing of **3APS_Ao** was carried out with the program DICVOL06[46] and the space group was assigned using the Smith and Snyder criteria.[47]

Differential Scanning Calorimetry (DSC). DSC measurements were performed using a Mettler Toledo DSC1 Excellence differential scanning calorimeter. The samples were weighed into aluminum DSC pans and crimped with a pinhole in the lid (samples mass ranges from 2 to 4 mg). Temperature and enthalpy calibrations were performed using indium as a standard. Melting point and heat of fusion (ΔH) were determined by measurements in the 300−470−300 K range at heating rates of 10 K/min. Experiments were performed in air. DSC peaks were analyzed using STAR^e software.[48] The melting data were calculated as the average of two measurements, and standard errors were ±0.1 K for temperature and ±0.3 kJ/mol for enthalpy.

Thermogravimetric Analysis (TGA). An EXSTAR Seiko 7200 analyzer was employed for thermogravimetric measurements (which were performed in duplicates). The experiments were performed at the rate of 10 K/min, from 300 to 870 K in air. The amount of sample in each TG measurement varied between 5 and 10 mg.

Hot-Stage Microscopy (HSM). Hot-stage microscopy measurements were carried out using a Leica DM2700 M device connected to a Linkam LTS350 platinum plate. Images were collected with the imaging software Leica Application Suite, from a Leica ICC50 W digital camera.

***In Silico* Analysis.** The crystal packing of the anhydrous and hydrate compounds was analyzed with Mercury.[43] CrystalExplorer 17[49] was used to compute the Hirshfeld surfaces (HSs) and their associated 2D fingerprint plots to further investigate the intermolecular interactions, which hold together the crystal of **3APS_0.5H$_2$Oo** and **3APS_Am** (data collected at 100 K).

https://doi.org/10.1021/acs.cgd.2c00849
Cryst. Growth Des. 2022, 22, 7176−7186

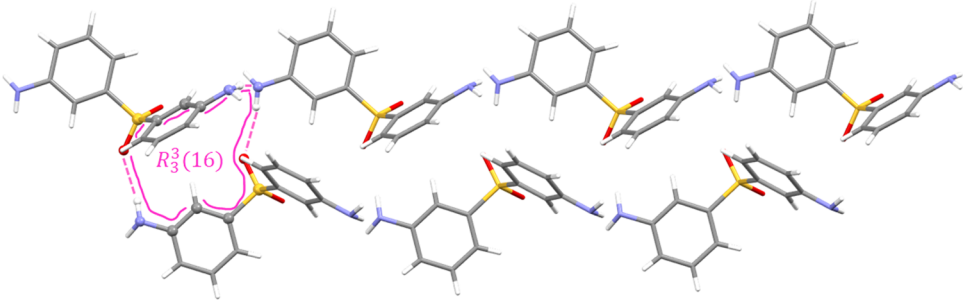

Figure 2. Crystal lattice of **3APS_0.5H$_2$Oo** (view along the *b*-axis): molecular chain made by H-bonded 3APS molecules.

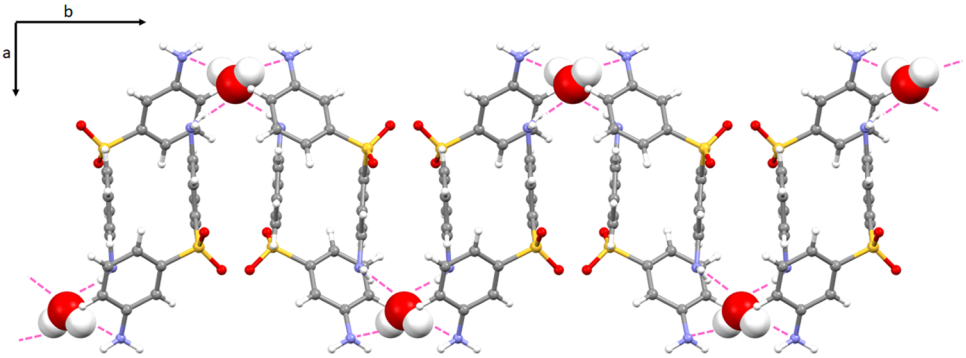

Figure 3. Crystal packing view of **3APS_0.5H$_2$Oo** highlighting the 3APS−water H-bonds within each ribbon.

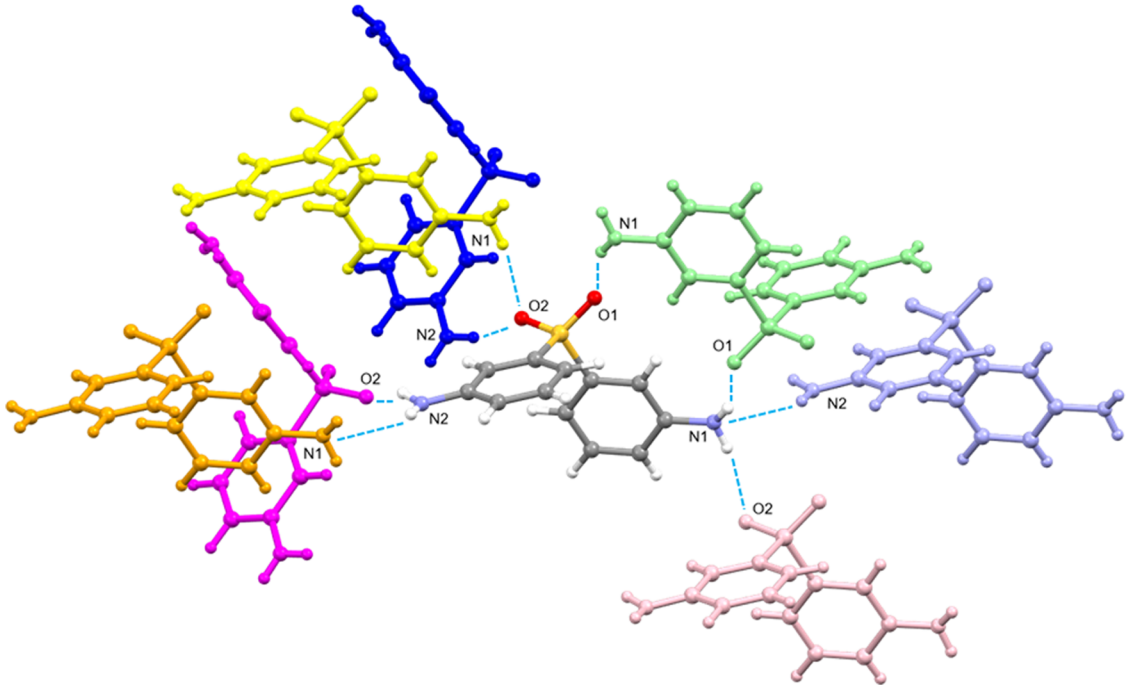

Figure 4. Intermolecular H-bonds involving each 3APS molecule in **3APS_Am**. Symmetry operation: pink = −1 + *x*, *y*, *z*; light green = 1 − *x*, 2−*y*,1−*z*; orange = 1 + *x*, −1 + *y*, *z*; violet = 1 − x,1 + *y*, *z*; magenta = 2 − *x*, −0.5 + *y*,1.5 − *z*; blue = 2 − *x*,0.5 + *y*,1.5 − *z*; yellow = 1 + *x*, *y*, −*z*.

RESULTS

Molecular and Crystal Structures from SCXRD. In the asymmetric unit of **3APS_0.5H$_2$Oo**, which crystallizes in the Pbna space group, one 3APS molecule and half a water molecule are present (the water oxygen atom O1w lies on a twofold rotation axis).

The overall shape adopted by the 3APS molecule in the hemihydrate species well compares with that observed in the anhydrous crystal forms: in all cases, the two −NH$_2$ groups are trans disposed with respect to the molecular backbone (Figure 1 right). Interestingly, this conformation is the only one observed in structures, deposited in the CSD, containing neutral 3APS molecules,[15,16,18,20] while in structures containing protonated 3APS molecules,[13−15,19,21] only the cis disposition has been found.

https://doi.org/10.1021/acs.cgd.2c00849
Cryst. Growth Des. 2022, 22, 7176−7186

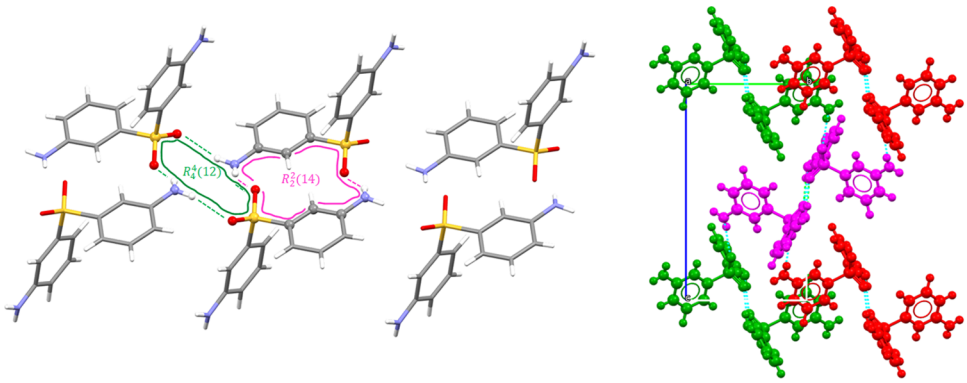

Figure 5. Crystal lattice of **3APS_Am**. Left: alternating $R_4^4(12)$ and $R_2^2(14)$ patterns within each molecular chain; right: molecular chains (magenta, green, and red) extending along the a-axis.

The angle (α) formed by the mean planes defined by the non-hydrogen atoms of the aromatic moieties in all four investigated 3APS solid forms is comparable to (see Table S2) and in agreement with the structural data deposited in the CSD for the fragment $SO_2(C_6H_2R_1R_2R_3)_2$ (only organic, 3D coordinates determined; no ortho substituents, acyclic sulfur).

As for the crystal packing, all of the H-bond acceptor and donor sites of the 3APS molecule contribute to its assembly (Figure S1), along with the water molecule, which is involved in four H-bonds with four sulfone molecules (symmetry related in pair through the twofold axis). As a whole, each 3APS molecule is H-bonded to six symmetry-related sulfone molecules, two for each $-SO_2$ and $-NH_2$ grouping and with two water molecules *via* the amine groups (see Table 2 for intermolecular bond distances and angles). As for the water molecule (*vide infra*, Discussion chapter), it acts as a H-bond acceptor to the N1 amine groups of two 3APS molecules (x,y,z and x, $1.5 - y$, $1 - z$) and as a H-bond donor toward the N2 atoms belonging to two further sulfone molecules ($1 - x$,$1 - y$, $1 - z$ and $1 - x$, $0.5 + y$, z).

In the crystal lattice, H-bonded 3APS molecules form chains, which extend along the *a*-axis direction (Figure 2). Within each chain, the $SO_2\cdots H_2N\cdots H_2N$ hydrogen bonds describe an $R_3^3(16)$ pattern,[50] while along the *b*-axis direction, the H-bonded 3APS−water molecules originate a ribbon (Figure 3) where the water molecules describe a zig-zag motif. Ribbons are interlinked *via* the sulfone molecules through hydrogen bonds involving the SO_2 and NH_2 groupings.

The *in silico* removal of the water molecules gives 2.9% of empty volume and shows that the water molecules are located in isolated voids (see Figure S2).

The dehydration process that leads to the formation of **3APS_0.1H$_2$Oo** suggests that, at least, a small quantity of water is fundamental to sustaining the observed crystal packing scaffold (*vide infra*, Discussion chapter).

In the anhydrous crystal form (**3APS_Am**), at variance with the hydrated species, the $-NH_2$ groups appear definitely less prone to acting as H-bond acceptors and consistently they are well in a plane (in contrast to the hydrated species, they are definitely pyramidal).[51] Each 3APS molecule is involved in eight strong H-bonds with seven symmetry-related molecules (see Table 2 and Figure 4) and in four quite weak ones (see Table 2). In the crystal lattice, centrosymmetric chains of 3APS molecules can be recognized, which extend parallel to the *a*-axis direction (Figure 5), with each chain being held together by $N(1)H_2\cdots O_2S$ hydrogen bonds, which originate alternating $R_2^2(14)$ and $R_4^4(12)$ patterns. Interchain $N(2)H_2\cdots O_2S$ H-bonds complete the intermolecular contacts.

Hirshfeld Surface Analysis. The Hirshfeld surface (HS) analysis and the related fingerprint plots were used to further analyze the intermolecular interactions in the 3APS crystal forms.

The most important intermolecular contacts described above show up as large deep-red depressions. Figures S3 and S4 show the HS of hydrated (**3APS_0.5H$_2$Oo**) and anhydrous (**3APS_Am**, 100 K) species together with the closest interacting species, respectively.[52] Both figures well evidence the unequal distribution of the H-bonded molecules around each 3APS molecule: the molecular shape of the 3APS molecule describes a sort of pocket, which is not interested in any intermolecular contact. The relative contributions to the Hirshfeld surface areas of **3APS_0.5H$_2$Oo** and **3APS_Am** due to O···H, N···H, C···H, and C···C interactions are very similar. However, a comparison of the related fingerprint plots (Figure S5) suggests that the $N\cdots H$ hydrogen bonds play different roles in stabilizing the crystal packing given that only in the hydrated species their contribution results in two characteristic sharp spikes (*vide infra*).

Temperature-Induced Phase Transformations. To investigate the temperature-dependent behavior of the 3APS solid forms, a set of different analyses was carried out using DSC, TGA, VT-PXRD, and HSM (in all cases, the temperature range was 100−470 K). Experiments were performed on **3APS_Am** and **3APS_0.5H$_2$Oo**.

3APS_Am. The PXRD pattern of a sample of 3APS, used as received without further purification, evidenced that the microcrystalline powder contains the anhydrous phase already described by Ghazisaeidi and Yousefi[16] (CSD refcode ROMCAY, **3APS_Am**; see Figure S6), whose crystal structure has been redetermined in the present work at 100 and 360 K.

The DSC curves of **3APS_Am** (Figure S7) (temperature range 300−460 K; rate 10 K/min during the heating step, 5 K/min during the cooling one, two cycles performed) showed one endothermic peak during the first heating stage, related to the melting of the compound at about 448 K (peak: 447.84 K; extrapolated peak: 447.84 K; enthalpy: 25.1 kJ/mol) followed, upon cooling the melt, by a recrystallization at 433 K (peak: 433.25 K; extrapolated peak: 433.14 K; enthalpy: 24.5 kJ/mol). During the second cycle, a similar behavior was observed.

Quite interestingly, the VT-PXRD analysis performed on the same sample (300−440 K range, two cycles performed) evidenced a slightly different behavior of the solid form. More

https://doi.org/10.1021/acs.cgd.2c00849
Cryst. Growth Des. 2022, 22, 7176−7186

in details, in agreement with what was observed in the DSC analysis, during the first heating step, the **3APS_Am** phase is stable until melting (see Figure S8). Cell parameters determined at different temperatures evidenced that **3APS_Am** underwent an anisotropic thermal expansion (see Table S3 reporting the thermal expansion coefficients, TECs).[53] More in particular (see Figure S9), while, as expected, the TEC values for *b* and *c* slightly increase with temperature; the opposite happens for *α*a. This behavior could be ascribed to the presence of a net of strong hydrogen bonds that link together 3APS molecules mostly along the *a* and *b* axes (see above).

At variance with the results from the DSC analysis, the PXRD pattern evidenced that during the first cooling step, between 410 and 370 K, a new orthorhombic crystalline phase, **3APS_Ao**, formed (its cell parameters were determined by PXRD data with the programs DICVOL06; **see** Table 3), which is stable at least between 370 and 300 K (Figure 6 and S10).

Table 3. Cell Parameters of 3APS_Ao Determined by PXRD Data

a (Å)	*b* (Å)	*c* (Å)	*V* (Å^3)	FOM	space group
25.02 (2)	11.57 (2)	7.983 (6)	2310.9 (3)	21.9	*Pbca*

3APS_Ao gave back the anhydrous **3APS_Am** phase on heating (temperature range 360−400 K; Figures S11 and S12).

3APS_0.5H$_2$Oo. Keeping in mind the result of the study on **3APS_Am**, a similar combined experiment (TGA, DSC, XRD) was carried out on **3APS_0.5H$_2$Oo**.

First of all, the crystalline phase of the powder was checked against that of the hydrated phase observed in single crystals, *i.e.*, **3APS_0.5H$_2$Oo** (see Figure S13).

Then, a DSC analysis was performed (temperature range 300−470 K; see Figure S14).

During the heating step, two endothermic peaks were observed: at 356 (peak: 356.8 K; extrapolated peak 356.5 K; enthalpy: 11.4 kJ/mol) and 447 K (peak: 446.1 K; extrapolated peak: 446.1 K; enthalpy: 23.1 kJ/mol).

To assign these peaks, a variable-temperature SCXRD analysis (VT-SCXRD) was carried out.

Cell parameters of a good-quality single crystal of **3APS_0.5H$_2$Oo** were determined at different temperature values (see Figure 7 and Table S4)

At each temperature, a short data acquisition was made, and the structure, as well as the occupancy of the water oxygen atom, was refined to determine the amount of water in the asymmetric unit. Results are summarized as follows: in the 100−340 K range, the 3APS:water ratio remained stable (2:1), while at 350 K, it was definitely higher (10:1). Thus, the partial dehydration of **3APS_0.5H$_2$Oo** occurred between 340 and 350 K (see Figure S14). At 360 K, the anhydrous **3APS_Am** monoclinic phase is formed, as evidenced by the cell values (a = 8.647(2), b = 8.810(9), c = 16.176(4) Å, β = 98.52(2)°): a sign that a single crystal-to-single crystal phase transition takes place, *i.e.*, the **3APS_0.1H$_2$Oo** → **3APS_Am** one (see Figure S15). TGA data evidence for the **3APS_0.1H$_2$Oo** species the loss of 1.1% of mass at about 358 K, in agreement with the formation of the anhydrous **3APS_Am** monoclinic phase.

The linear (α) and volume (β) thermal expansion coefficients (TECs), calculated for **3APS_0.5H$_2$Oo** in the 100−340 K range (taking as reference the cell parameter values at 100 K, Table S5), evidenced that on increasing the temperature, this phase underwent a slightly anisotropic expansion with the a-axis length almost constant until 330 K and definitely decreasing on approaching 340 K, *i.e.*, close to the temperature where partial dehydration occurred.

To conclude, DSC, XRD, and TGA combined experiments evidenced that:

(1) **3APS_0.5H$_2$Oo** is stable from 100 to 330 K;
(2) between 340 and 350 K, the partial loss of water molecules resulted in the partially hydrated form **3APS_0.1H$_2$Oo**;
(3) at 360 K, **3APS_0.1H$_2$Oo** completely leaked water and the anhydrous **3APS_Am** was formed;
(4) **3APS_Am** is stable from 100 K to melting;
(5) on cooling down the melt **3APS_Am** (at least in the VT-PXRD experiment), a second anhydrous phase, **3APS_Ao**, formed (between 410 and 370 K), which is stable until 300 K; and
(6) on increasing the temperature, between 360 and 400 K, its single crystal-to-single crystal transition to **3APS_Am** was observed.

Finally, polarized light HSM was used to visualize the sample changes related to each single crystal-to-single crystal phase transition.

As reported above, heating induced the partial dehydration of **3APS_0.5H$_2$Oo** at temperatures slightly above 350 K (Figure 8-top); the process is clearly visible, being characterized by the

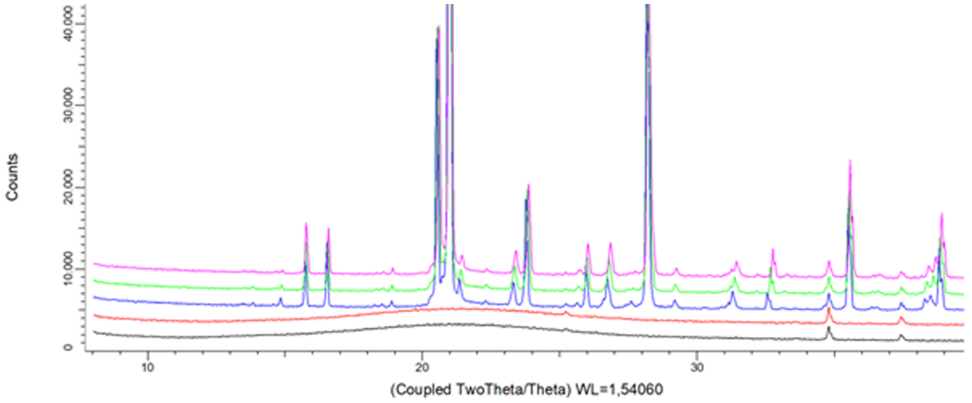

Figure 6. Superimposition of the PXRD pattern collected during the first cooling step of the VT-PXRD experiment on **3APS_Am** at 440 K (black), 410 K (red), 370 K (blue), 330 K (green), and 300 K (magenta).

https://doi.org/10.1021/acs.cgd.2c00849
Cryst. Growth Des. 2022, 22, 7176−7186

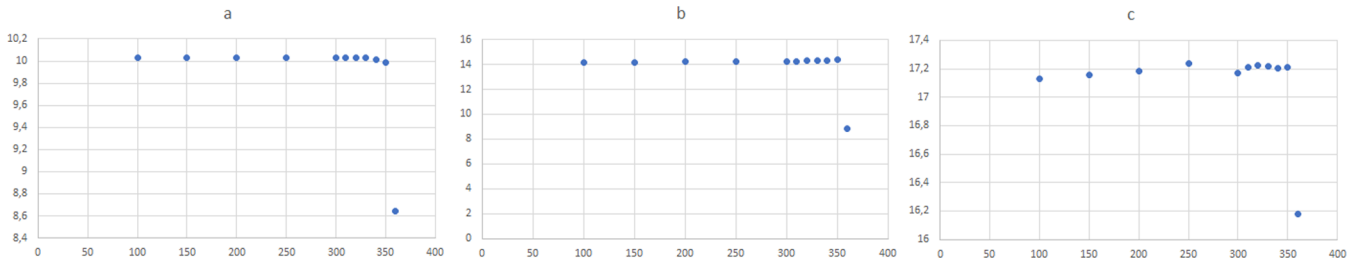

Figure 7. Plots of a, b, and c cell lengths monitored at different temperatures during the **3APS_0.5H$_2$Oo -> 3APS_0.1H$_2$Oo-> 3APS_Am**. Left: a; middle: b; right: c.

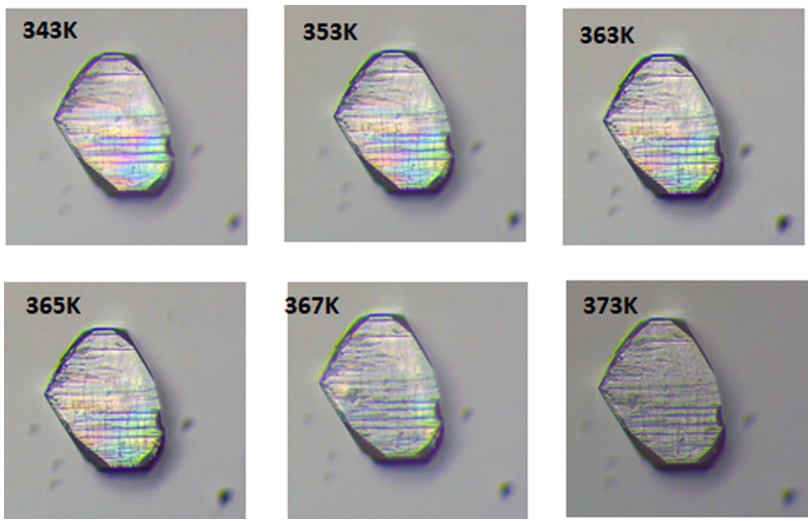

Figure 8. Polarized light hot-stage microscopy images of 3APS. Top: **3APS_0.5H$_2$Oo → 3APS_0.1H$_2$Oo** partial dehydration process. Bottom: **3APS_0.1H$_2$Oo → 3APS_Am** single crystal-to-single crystal transformation.

Scheme 2. Scheme of the Relationships between Crystalline Phases of 3APS Here Reported

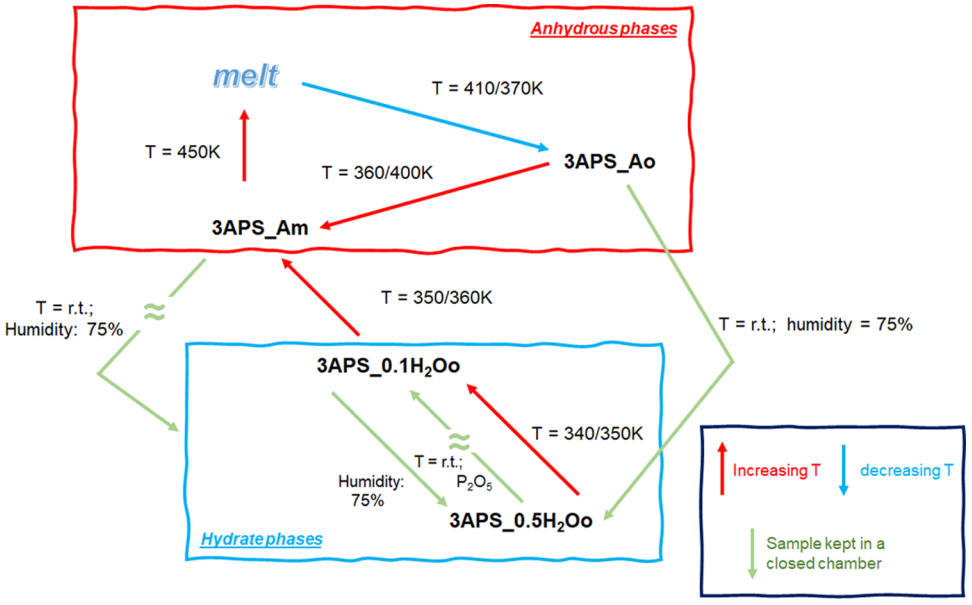

formation of cracks in the crystal structure due to the partial loss of water molecules.

Subsequently, the increasing temperature leads to a single crystal-to-single crystal transformation of **3APS_0.1H$_2$Oo** into **3APS_Am** (Figure 8-bottom) between 360 and 370 K. This transformation is indicated by changes in interference colors. The pronounced changes in texture that accompany the transformation **3APS_0.1H$_2$Oo → 3APS_Am** evidenced that, in comparison to the dehydration process of **3APS_0.5H$_2$Oo** that ends with **3APS_0.1H$_2$Oo**, a greater structural rearrangement occurred.

https://doi.org/10.1021/acs.cgd.2c00849
Cryst. Growth Des. 2022, 22, 7176−7186

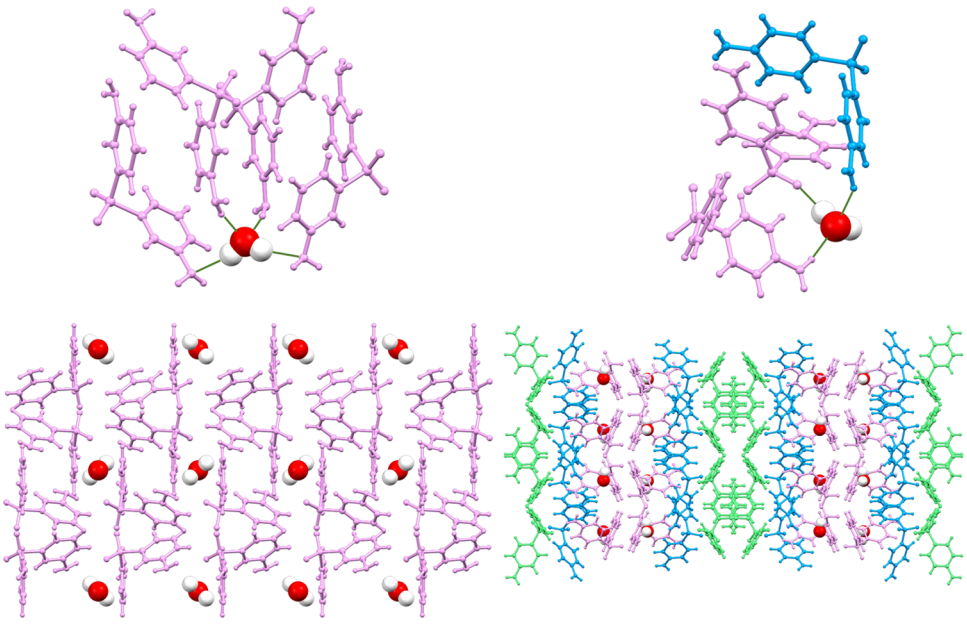

Figure 9. Top: left: 3APS−water interactions in **3APS_0.5H$_2$Oo**; right: 4APS-water interactions in **4APS_0.33H$_2$Om** (CSD refcode: ANSFON02). Bottom: left: **3APS_0.5H$_2$Oo** crystal packing; right: **4APS_0.33H$_2$Om** crystal packing (molecules that do not interact with water, labeled as C in the article by Braun and Griesser,[35] are in light green).

Phase Stability Tests. **3APS_0.5H$_2$Oo** crystals were found to be stable, *i.e.*, they do not dehydrate, even when kept in a closed chamber in the presence of P_2O_5 at rt for several days.

Crystals of **3APS_0.1H$_2$Oo** (obtained by heating **3APS_0.5H$_2$Oo** crystals to 350 K and monitoring the **3APS_0.5H$_2$Oo** → **3APS_0.1H$_2$Oo** dehydration by SCXRD analysis) were stable at room temperature for at least two days, but they quickly rehydrate if put in a closed chamber at rt and constant humidity (ca. 75% using a saturated solution of NaCl).

3APS_Ao, when kept for one day in the same conditions of **3APS_0.1H$_2$Oo** (closed chamber at rt and ca. 75% humidity using a saturated solution of NaCl), is able to hydrate and, as evidenced by the PXRD pattern collected at the end of the experiment, the **3APS_0.5H$_2$Oo** phase is formed (see Figure S16).

By contrast, the **3APS_Am** phase did not hydrate if kept in the same conditions as above nor if the experiment lasted a week.

DISCUSSION

About a third of all of the known organic molecules exist as different hydrated forms.[54] This may depend on the fact that water molecules, due to their small size and to their capability to give multiple hydrogen bonds, are ideal to link together organic molecules in stable crystal structures.[55]

Hydrated compounds, depending on the storage conditions (RH and temperature, for example), may undergo dehydration processes, which can lead to the formation of different hydrated species, with a different amount of water, or to anhydrous compounds (both crystalline or amorphous phases) given that the dehydration and rehydration processes can be very complex; the study of the different hydrated phases of a given organic molecule, their transformation, and their mutual interrelationship are of fundamental importance to foresee/avoid problems related to storage *vs* properties of the investigated substance. The above-reported experiments were undertaken with the aim to better understand the relationship between anhydrous 3APS phases, **3APS_Am** and **3APS_Ao**, and the partially hydrated ones also in comparison with the solid forms' behavior of the strictly related compound dapsone.

In Scheme 2, the relationships between all of the known crystalline phases of 3APS are reported.

In **3APS_0.5H$_2$Oo**, the water molecules are located in isolated voids (see Results, Molecular and Crystal Structures from SCXRD paragraph and Figure S2), and this hydrate can be classified as an isolated site one.[56] The same occurs in the 0.33 hydrate dapsone phase (**4APS_0.33H$_2$Om**, in the following), as provided by the crystal structure deposited in the CSD (refcodes = ANSFON, ANSFON01, and ANSFON02). In **4APS_0.33H$_2$O**, only two out of the three crystallographically independent 4APS molecules interact with the water molecules (see Figure 9). As a consequence, excluding the 4APS molecule not interacting with water, both the hydrates (**3APS_0.5H$_2$Oo** and **4APS_0.33H2Om**) show the same API/water ratio, *i.e.*, 2:1. However, a difference occurs; in fact, the water environment can be classified as a DDAA type (A, hydrogen-bonding acceptor; D, hydrogen-bonding donor)[57] in **3APS_0.5H$_2$Oo**, while in **4APS_0.33H2Om**, the water molecules belong to the DAA type. This means that, in the 3APS hydrated species, the water molecule uses all its donor and acceptor potentialities, at variance with the hydrated dapsone, where the donor potentialities are not fully exploited. In addition, the water molecule acts as a H-bond donor toward two different kinds of acceptors: the $-NH_2$ nitrogen and the $-SO_2$ oxygen atoms in **3APS_0.5H$_2$Oo** (see also the Hirshfeld Surface Analysis section) and **4APS_0.33H2Om**, respectively. This different behavior may be attributed to the different charge distribution of the $-NH_2$ nitrogen and $-SO_2$ oxygen atoms in 3APS vs 4APS of the group, which reflects their H-bond-accepting ability.

On this basis, we can speculate that the crystallization water molecules play a different role in stabilizing the crystal packing of the two strictly related compounds, which in turn reflects their different behavior in the hydration/dehydration process, which is stoichiometric for **3APS_0.5H$_2$Oo** and, quite surprisingly,

https://doi.org/10.1021/acs.cgd.2c00849
Cryst. Growth Des. 2022, 22, 7176−7186

nonstoichiometric for **4APS_0.33H$_2$Om**. In fact, as reported by Braun and Griesser,[35] on the basis of the hydration/dehydration mechanisms and the subsequent structural changes, hydrated compounds may be classified as *stoichiometric*, *i.e.*, compounds that show a well-defined water content at a given relative humidity and, generally, whose dehydration involves a considerable rearrangement of the host molecules, and *non-stoichiometric* hydrates. Compounds belonging to this second class usually present channels in their crystal packing where the water molecules are lodged, often rather weakly bonded. Water molecules can fully or partly escape through these channels, giving rise to an anhydrous species without significant changes in the crystal structure. In their work on the **4APS_0.33H$_2$Om** compound, Braun and Griesser[35] proved that this compound, although its water molecule is confined in isolated sites, belongs to the *nonstoichiometric* hydrate group. In fact, DSC results showed that a complete loss of water, induced by temperature, occurs in the 310−360 K range (where a broad endothermic event was observed), leading to an identical anhydrous phase, which then transformed in phase II at about 380 K. In the case of 3APS, something different occurred, *i.e.*, an anhydrous isomorphic phase was not observed during the dehydration process. Instead, the dehydration proceeded through a partial loss of the water content, leading to the partially hydrated **3APS_0.1H$_2$Oo**; the complete removal of the water molecules results in a single crystal-to-single crystal transition from orthorhombic to monoclinic. Then, we can speculate that the water molecules present in the crystal packing of the orthorhombic hydrated phases (even if in a very low quantity) are fundamental for the existence of the crystal packing, and their complete removal induced a structural rearrangement, leading to a different disposition of the 3APS molecules and a different net of interactions.

As a consequence, the **3APS_0.5H$_2$Oo** compound can be classified as a "true" stoichiometric hydrate, also on the basis of its dehydration behavior. In addition, the analysis of the linear (α) and volume (β) thermal expansion coefficients (TECs) (see Table S5) calculated in the 150−340 K range (taking as reference the cell parameter values at 100 K) can help in understanding the dehydration mechanism. In fact, as evidenced in Tables S4 and S5, on increasing the temperature, the hemihydrated phase underwent a slightly anisotropic expansion being the length of the *a*-axis almost identical until 330 K, while its value significantly decreased on approaching 340 K, where the stable partial hydrate **3APS_0.1H$_2$Oo** was observed. With this in mind, and considering that, as reported in the "Molecular and Crystal Structures from SCXRD" paragraph, along the *a*-axis direction chains made of H-bonded 3APS molecules are present, we can speculate that the loss of water molecules may be due to the expansion of the distances between these chains subsequent to the increase in temperature (see Scheme 3).

Finally, concerning the anhydrous phase **3APS_Ao**, although its solid-state structure was not determined, some useful information has been retrieved by means of VT-PXRD analysis and hydration−dehydration experiments carried out at constant humidity. The **3APS_Ao** phase is observed only during the cooling step of a VT-PXRD and, although it is stable at room temperature, it quickly hydrated, to **3APS_0.5H$_2$Oo**, when kept in a closed chamber at constant humidity (ca. 75% using a saturated solution of NaCl). In addition, on heating the sample to 360−400 K, the **3APS_Ao** → **3APS_Am** transition is observed. Given the possibility of **3APS_Ao** to convert to **3APS_Am** at a given temperature through a solid−solid phase transition, the two anhydrous solid forms can be categorized as enantiotropic polymorphs.[58] In addition, the orthorhombic phase seems to be the kinetically preferred one (it crystallizes from the 3APS melt), being the already known **3APS_Am** the thermally most stable (**3APS_Ao** transforms in **3APS_Am** by increasing the temperature to 360/400 K).

Scheme 3. Schematic Representation of the Proposed Mechanism for the 3APS_0.5H$_2$Oo Dehydration Process

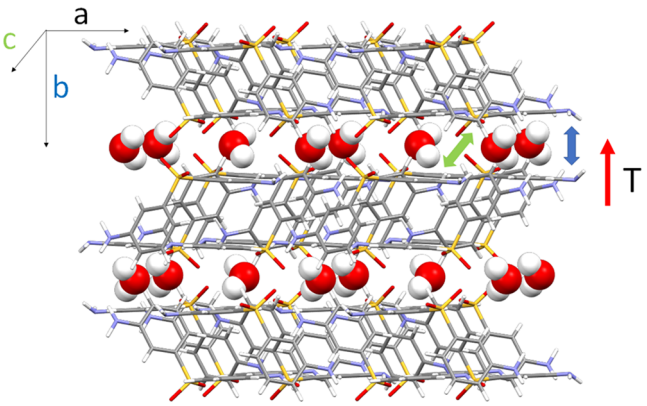

CONCLUSIONS

In this paper, we have presented the results of a solid-state investigation of different anhydrous and hydrated species of a dapsone-related molecule, *i.e.*, 3,3′-diaminophenyl sulfone (3APS). Three of the four reported species (the partially hydrated ones and the orthorhombic anhydrous phase **3APS_Ao**) were observed for the first time. VT-PXRD, DSC, TGA, and HSM experiments, as well as *in silico* analysis, were used to investigate their solid behavior and the interconversion between the different phases. Finally, a comparison of the dehydration processes of the **3APS_0.5H$_2$O** compound with the related **4APS_0.33H$_2$Om** was undertaken to clarify/rationalize the different dehydration behavior observed in 3APS and 4APS, which can be classified as stoichiometric and nonstoichiometric hydrated, respectively.

ASSOCIATED CONTENT

Supporting Information

The Supporting Information is available free of charge at https://pubs.acs.org/doi/10.1021/acs.cgd.2c00849.

CIF Files of **3APS_Am** (data collected at 100 and 360 K), **3APS_0.5H$_2$Oo**, and **3APS_0.1H$_2$Oo**; views of the Hirshfeld surfaces and fingerprint plots of **3APS_Am** and **3APS_0.5H$_2$Oo**; and DSC of **3APS_Am** and **3APS_0.5H$_2$Oo;**; PXRD patterns; and; tables containing linear and volume thermal expansion coefficients calculated for **3APS_0.5H$_2$Oo** (PDF)

Accession Codes

CCDC 2193055−2193058 contain the supplementary crystallographic data for this paper. These data can be obtained free of charge via www.ccdc.cam.ac.uk/data_request/cif, or by emailing data_request@ccdc.cam.ac.uk, or by contacting The Cambridge Crystallographic Data Centre, 12 Union Road, Cambridge CB2 1EZ, UK; fax: +44 1223 336033.

https://doi.org/10.1021/acs.cgd.2c00849
Cryst. Growth Des. 2022, 22, 7176−7186

AUTHOR INFORMATION

Corresponding Author

Patrizia Rossi − *Department of Industrial Engineering, University of Florence, Florence 50139, Italy;* orcid.org/0000-0002-6316-338X; Email: p.rossi@unifi.it

Authors

Paola Paoli − *Department of Industrial Engineering, University of Florence, Florence 50139, Italy;* orcid.org/0000-0002-2408-4590

Martina Lippi − *Department of Industrial Engineering, University of Florence, Florence 50139, Italy*

Stella Milazzo − *Department of Industrial Engineering, University of Florence, Florence 50139, Italy;* Present Address: Takeda Baxter Manufacturing, via Giovan Battista Oliva 2, Pisa 56121, Italy

Jacopo Ceccarelli − *Department of Industrial Engineering, University of Florence, Florence 50139, Italy;* Present Address: Department of Experimental and Clinical Medicine, Largo Brambilla 3, Florence 50134, Italy; orcid.org/0000-0002-0759-787X

Laura Chelazzi − *Centro di Cristallografia Strutturale, University of Florence, Sesto F.no (Florence) 50019, Italy*

Andrea Ienco − *Consiglio Nazionale delle Ricerche, Istituto di Chimica dei Composti OrganoMetallici (CNR-ICCOM), Sesto F.no (Florence) 50019, Italy;* orcid.org/0000-0002-2586-4943

Luca Conti − *Department of Chemistry "U. Schiff", University of Florence, Sesto F.no (Florence) 50019, Italy;* orcid.org/0000-0002-0402-1293

Complete contact information is available at: https://pubs.acs.org/10.1021/acs.cgd.2c00849

Author Contributions

The manuscript was written through contributions of all authors. All authors have given approval to the final version of the manuscript.

Notes

The authors declare no competing financial interest.

ACKNOWLEDGMENTS

The authors would like to thank the Centro di Cristallografia Strutturale (CRIST) of the University of Firenze for the X-ray diffraction facilities and Dr Samuele Ciattini for his valuable technical assistance. Elisa Passaglia (ICCOM-CNR, Pisa), who performed the TGA analysis, is also kindly acknowledged.

ABBREVIATIONS USED

3APS =3,3′-diaminophenyl sulfone; 4APS =4,4′-diaminophenyl sulfone = dapsone; XRD =X-ray diffraction; SCXRD =single-crystal X-ray diffraction; PXRD =powder X-ray diffraction; VT-XRD =variable-temperature X-ray diffraction; DSC =differential scanning calorimetry; TGA =thermogravimetric analysis; HSM =hot-stage microscopy

REFERENCES

(1) Irshad, A.; Shagufta. Sulfones: an important class of organic compounds with diverse biological activities. *Int. J. Pharm. Pharm. Sci.* **2015**, *7*, 19−27.

(2) Ue, M.; Sasaki, Y.; Tanaka, Y.; Morita, M. Nonaqueous electrolytes with advances in solvents. In *Electrolytes for Lithium and LithiumIon Batteries*; Jow, T. R.; Xu, K.; Borodin, O.; Ue, M., Eds.; Springer: New York, 2014; pp 93−165.

(3) Trost, B. M.; Kalnmals, C. A. Sulfones as chemical chameleons: versatile synthetic equivalents of small-molecule synthons. *Chem. − Eur. J.* **2019**, *25*, 11193−11213.

(4) McMahon, J. B.; Gulakowski, R. J.; Weislow, O. S.; Schultz, R. J.; Narayanan, V. L.; Clanton, D. J.; Pedemonte, R.; Wassmundt, F. W.; Buckheit, R. W.; Decker, W. D. Diarylsulfones, a New Chemical Class of Nonnucleoside Antiviral Inhibitors of Human Immunodeficiency Virus Type 1 Reverse Transcriptase. *Antimicrob. Agents Chemother* **1993**, *37*, 754−760.

(5) Teall, M.; Oakley, P.; Harrison, T.; Shaw, D.; Kay, E.; Elliott, J.; Gerhard, U.; Castro, J. L.; Shearman, M.; Ball, R. G.; Tsou, N. N. Aryl sulfones: a new class of γ-secretase inhibitors. *Bioorg. Med. Chem. Lett* **2005**, *15*, 2685−2688.

(6) Biswas, K.; Aya, T.; Qian, W.; Peterkin, T. A. N.; Chen, J. J.; Humana, J.; Hungate, R. W.; Kumar, G.; Arik, L.; Lester-Zeiner, D.; Biddlecome, G.; Manning, B. H.; Sun, H.; Dong, H.; Huang, M.; Loeloff, R.; Johnson, J. E.; Askew, B. C. Aryl sulfones as novel Bradykinin B1 receptor antagonists for treatment of chronic pain. *Bioorg. Med. Chem. Lett* **2008**, *18*, 4764−4769.

(7) Wozel, G.; Blasum, C. Dapsone in dermatology and beyond. *Arch Dermatol Res* **2014**, *306*, 103−124.

(8) Kanwar, B. A.; Khattak, A.; Balentine, J.; Lee, J. H.; Kast, R. E. *Vaccines* **2022**, *26*, 195.

(9) Braun, D. E.; Gelbrich, T.; Griesser, U. J. Experimental and computational approaches to produce and characterize isostructural solvates. *CrystEngComm* **2019**, *21*, 5533−5545.

(10) Braun, D. E.; Krüger, H.; Kahlenberg, V.; Griesser, U. J. Molecular level understanding of the reversible phase transformation between forms III and II of dapsone. *Cryst. Growth Des.* **2017**, *17*, 5054−5060.

(11) Zhang, Q.-L.; Hu, P.; Zhao, Y.; Feng, G.; Zhang, Y.; Zhu, B.; Tao, Z. Anion-controlled assembly of silver-di(aminophenyl)sulfone coordination polymers: Syntheses, crystal structures, and solid-state luminescence. *J. Solid State Chem.* **2014**, *210*, 178−187.

(12) Rudyk, H.; Knaggs, M. H.; Vasiljevic, S.; Hope, J.; Birkett, C.; Gilbert, I. H. Synthesis and evaluation of analogues of Congo red as potential compounds against transmissible spongiform encephalopathies. *Eur. J. Med. Chem.* **2003**, *38*, 567−579.

(13) Kessentini, A.; Dammak, T.; Belhouchet, M. Synthesis, molecular structure, vibrational spectroscopy, optical investigation and DFT study of a novel hybrid material: 3,3′- diammoniumdiphenylsulfone hexachloridostannate monohydrate. *J. Mol. Struct.* **2017**, *1149*, 818−827.

(14) Mahroug, A.; Belhouchet, M.; Hémon-Ribaus, A.; Mhiri, T. Synthesis, Crystal Structure, and Characterization of a New Adduct3-Ammoniumphenyl Sulfone Dihydrogenphosphate Phosphoric Acid $[C_{12}H_{14}N_2SO_2]$ $(H_2PO_4)2$ H_3PO_4. *Phosphorus, Sulfur Silicon Relat. Elem.* **2011**, *186*, 2332−2340.

(15) Mahroug, A.; Belhouchet, M.; Mhiri, T. Synthesis, Crystal Structure, and Characterization of a New Hydrogen Phosphate Templated By 3-Aminophenyl Sulfone. *Phosphorus, Sulfur Silicon Relat. Elem.* **2012**, *187*, 1482−1489.

(16) Ghazisaeidi, R.; Yousefi, M. 3-(3-Aminophenylsulfonyl) aniline. *Acta Crystallogr., Sect. E: Crystallogr. Commun.* **2009**, *65*, o222.

(17) Groom, C. R.; Bruno, I. J.; Lightfoot, M. P.; Ward, S. C. The Cambridge Structural Database. *Acta Crystallogr., Sect. B: Struct. Sci., Cryst. Eng. Mater.* **2016**, *72*, 171−179.

(18) Rudolph, F. A. M.; Fuller, A. M.; Slawin, A. M. Z.; Buhl, M.; Aitken, R. A.; Woollins, J. D. The X-ray Structures of Sulfones. *J Chem Crystallogr.* **2010**, *40*, 253−265.

(19) Bouguerra, M.; Mahroug, A.; Wróbel, A.; Trzybiński, D.; Woźniak, K.; Belhouchet, M. Physico-chemical study of new supramolecular-architectured hybrid organic−inorganic sulfates incorporating diammoniumdiphenylsulfone cations. *RSC Adv.* **2021**, *11*, 26368−26378.

(20) Yao, W.; Li, F.-S.; Yu, D.-S.; Lu, C.; Zhu, J.-N. Bis(3-aminophenyl) sulfone acetonitrile solvate. *Acta Cystallogr., Sect. E: Struct. Rep. Online* **2008**, *64*, o1140.

(21) Ltaief, H.; Mahroug, A.; Paoli, P.; Rossi, P.; Belhouchet, M. A new hybrid compound based on mercury and 3,3′-diaminobiphenylsulfone studied by a combined experimental and theoretical approach. *J. Mol. Struct.* **2020**, *1220*, No. 128760.
(22) Rossi, P.; Paoli, P.; Chelazzi, L.; Conti, L.; Bencini, A. The solid-state structure of the β-blocker metoprolol: a combined experimental and in silico investigation. *Acta Crystallogr., Sect. C: Struct. Chem.* **2019**, *C75*, 87−96.
(23) Paoli, P.; Rossi, P.; Macedi, E.; Ienco, A.; Chelazzi, L.; Bartolucci, G. L.; Bruni, B. Similar but Different: The Case of Metoprolol Tartrate and Succinate Salts. *Cryst. Growth Des.* **2016**, *16*, 789−799.
(24) Rossi, P.; Paoli, P.; Chelazzi, L.; Conti, L.; Bencini, A. Metroprolol Fumarate: Crystal Structure from Powder X-ray Diffraction Data and Comparison with the Tartrate and Succinate Salts. *Cryst. Growth Des.* **2018**, *18*, 7015−7026.
(25) Paoli, P.; Milazzo, S.; Rossi, P.; Ienco, A. Rationalization of Lattice Thermal Expansion for Beta-Blocker Organic Crystals. *Crystals* **2020**, *10*, 350.
(26) Rossi, P.; Ceccarelli, J.; Milazzo, S.; Paoli, P.; Ciattini, S.; Ienco, A.; Tuci, G.; Morais Missina, J.; Valleri, M.; Giovannoni, M. P.; Guerrini, G.; Conti, L. NSAIDs − 1-phenylethylamine diastereomeric salts: a systematic solid-state investigation. *Cryst. Growth Des.* **2021**, *21*, 6947−6960.
(27) Morais Missina, J.; Conti, L.; Rossi, P.; Ienco, A.; Gioppo Nunes, G.; Valtancoli, B.; Chelazzi, L.; Paoli, P. Ibuprofen as linker for calcium(II) in a 1D-coordination polymer: A solid state investigation complemented with solution studies. *Inorg. Chim. Acta* **2021**, *523*, 120319−120320.
(28) Rossi, P.; Macedi, E.; Paoli, P.; Bernazzani, L.; Carignani, E.; Borsacchi, S.; Geppi, M. Solid−Solid Transition between Hydrated Racemic Compound and Anhydrous Conglomerate in Na-Ibuprofen: A Combined X-ray Diffraction, Solid-State NMR, Calorimetric, and Computational Study. *Cryst. Growth Des.* **2014**, *14*, 2441−2452.
(29) Rossi, P.; Paoli, P.; Chelazzi, L.; Milazzo, S.; Biagi, D.; Valleri, M.; Ienco, A.; Valtancoli, B.; Conti, L. Relationships between Anhydrous and Solvated Species of Dexketoprofen Trometamol: A Solid-State Point of View. *Cryst. Growth Des.* **2020**, *20*, 226−336.
(30) Rossi, P.; Paoli, P.; Milazzo, S.; Chelazzi, L.; Giovannoni, M. P.; Guerrini, G.; Ienco, A.; Valleri, M.; Conti, L. A combined crystallographic and computational study on dexketoprofen trometamol dihydrate salt. *Crystals* **2020**, *10*, 659−672.
(31) Paoli, P.; Rossi, P.; Chelazzi, L.; Altamura, M.; Fedi, V.; Giannotti, D. Solid State Investigation and Characterization of a Nepadutant Precursor: Polymorphic and Pseudopolymorphic Forms of MEN11282. *Cryst. Growth Des.* **2016**, *16*, 5294−5304.
(32) Rossi, P.; Paoli, P.; Ienco, A.; Biagi, D.; Valleri, M.; Conti, L. A new crystal form of the NSAID dexketoprofen. *Acta Crystallogr., Sect. C: Struct. Chem.* **2019**, *75*, 783−792.
(33) Rossi, P.; Paoli, P.; Milazzo, S.; Chelazzi, L.; Ienco, A.; Conti, L. Investigating differences and similarities between betaxolol polymorphs. *Crystals* **2019**, *9*, 509−521.
(34) Araya-Sibaja, A. M.; Fandaruff, C.; Guerava-Camargo, A. M.; Vargas-Huertas, F.; Zamora, W. J.; Vega-Baudrit, J. R.; Guillén-Giron, T.; Navarro-Hoyos, M.; Paoli, P.; Rossi, P.; Jones, W. Crystal forms of the antihypertensive drug Irbesartan: a crystallographic, spe3ctroscopic, and Hirshfeld surface analysis investigation. *ACS Omega* **2022**, *7*, 14897−14909.
(35) Braun, D. E.; Griesser, U. J. Supramolecular Organization of Nonstoichiometric Drug Hydrates: Dapsone. *Front. Chem* **2018**, *6*, No. 31.
(36) Bruker *Bruker APEX2*; Bruker AXS Inc.: Madison, Wisconsin, USA, 2012.
(37) Bruker *Bruker SAINT*; Bruker AXS Inc.: Madison, Wisconsin, USA, 2012.
(38) Krause, L.; Herbst-Irmer, R.; Sheldrick, G. M.; Stalke, D. Comparison of silver and molybdenum microfocus X-ray sources for single-crystal structure determination. *J. Appl. Cryst.* **2015**, *48*, 3−10.
(39) Burla, M. C.; Caliandro, R.; Camalli, M.; Carrozzini, B.; Cascarano, G. L.; Da Caro, L.; Giacovazzo, C.; Polidori, G.; Spagna, R. An improved tool for crystal structure determination and refinement. *J. Appl. Crystallogr.* **2005**, *38*, 381−388.
(40) Sheldrick, G. M. Crystal structure refinement with *SHELXL*. *Acta Crystallogr., Sect. C: Struct. Chem.* **2015**, *71*, 3−8.
(41) Nardelli, M. *PARST95* - an update to *PARST*: a system of Fortran routines for calculating molecular structure parameters from the results of crystal structure analyses. *J. Appl. Crystallogr.* **1995**, *28*, 659.
(42) Farrugia, L. J. *ORTEP*-3 for Windows - a version of *ORTEP*-III with a Graphical User Interface (GUI). *J. Appl. Crystallogr.* **1997**, *30*, 565.
(43) Macrae, C. F.; Bruno, I. J.; Chisholm, J. A.; Edgington, P. R.; McCabe, P.; Pidcock, E.; Rodriguez-Monge, E.; Taylor, R.; van de Streek, J.; Wood, P. A. New Features for the Visualization and Investigation of Crystal Structures. *J. Appl. Crystallogr.* **2008**, *41*, 466−470.
(44) Dassault Systèmes BIOVIA. *Discovery Visualizer, v19.1.0.18287*; Dassault Systèmes: San Diego, 2019.
(45) Toby, B. H.; Von Dreele, R. B. GSAS-II: the genesis of a modern open-source all purpose crystallography software package. *J. Appl. Crystallogr.* **2013**, *46*, 544−549.
(46) Boultif, A.; Louë r, D. Powder pattern indexing with the dichotomy method. *J. Appl. Crystallogr.* **2004**, *37*, 724−731.
(47) Smith, G. S.; Snyder, R. L. FN: A criterion for rating powder diffraction patterns and evaluating the reliability of powder-pattern indexing. *J. Appl. Crystallogr.* **1979**, *12*, 60−65.
(48) STARe. *Thermal Analysis Software*; Mettler - Toledo Int. Inc.: Sonnenbergstrasse 74 − CH-8603Schwerzenbahc, Switzerland.
(49) Turner, M. J.; McKinnon, J. J.; Wolff, S. K.; Grimwood, D. J.; Spackman, P. R.; Jayatilaka, D.; Spackman, M. A. *Crystal Explorer17*; University of Western Australia, 2017.
(50) Etter, M. C.; MacDonald, J. C.; Bernstein, J. Graph-set analysis of hydrogen-bond patterns in organic crystals. *Acta Crystallogr., Sect. B: Struct. Sci.* **1990**, *46*, 256−262.
(51) The sum of the angles around N1 and N2 are: 338, 343° and 351, 358° for **3APS_0.5H$_2$Oo** and **3APS_Am**, respectively.
(52) The lack of hydrogen atoms on the water molecule in **3APS_0.1H$_2$Oo** prevents its analysis with CrystalExplorer.
(53) TECs = $\alpha = \frac{1}{l_{T=0}} \cdot \frac{\Delta l}{\Delta T}$ and $\beta = \frac{1}{V_{T=0}} \cdot \frac{\Delta V}{\Delta T}$ (see: (a) Hori, R.; Sugiyama, J.; Wada, M.; et al. *Carbohydr. Polym.* **2007**, *70*, 298−303. (b) Krishnan, R. S.; Srinivasan, R.; Devanarayanan, S. *Thermal Expansion of Crystals*; Pergamon, 1979.
(54) Braun, D. E.; Griesser, U. J. Stoichiometric and Non-stoichiometric Hydrates of Brucine. *Cryst. Growth Des.* **2016**, *16*, 6111−6121.
(55) Vippagunta, S. R.; Brittain, H. G.; Grant, D. J. W. Crystalline solids. *Adv. Drug Delivery Rev.* **2001**, *48*, 3−26.
(56) Byrn, S. R.; Zografi, G.; Chen, X. *Solid-State Properties of Pharmaceutical Materials*; Wiley: Hoboken, NJ, 2017.
(57) Infantes, L.; Fabian, L.; Motherwell, W. D. S. Organic crystal hydrates: what are the important factors for formation. *CrystyEngomm* **2007**, *9*, 65−71.
(58) Kawakami, K. Reversibility of Enantiotropically Related Polymorphic Transformations from a Practical Viewpoint: Thermal Analysis of Kinetically Reversible/Irreversible Polymorphic Transformations. *J. Pharm. Sci.* **2007**, *96*, 982−989.

https://doi.org/10.1021/acs.cgd.2c00849
Cryst. Growth Des. 2022, 22, 7176−7186